Extreme Mechanics Letters 17 (2017) 24–32

Contents lists available at ScienceDirect

Extreme Mechanics Letters

journal homepage: www.elsevier.com/locate/eml

Broadband and multiband vibration mitigation in lattice metamaterials with sinusoidally-shaped ligaments

Yanyu Chen [a], Feng Qian [b], Lei Zuo [b], Fabrizio Scarpa [c], Lifeng Wang [a,*]

[a] Department of Mechanical Engineering, State University of New York at Stony Brook, Stony Brook, NY 11794, USA
[b] Department of Mechanical Engineering, Virginia Tech, Blacksburg, VA 24061, USA
[c] Advanced Composites Centre for Innovation and Science, University of Bristol, Bristol, BS8 1TR, UK

GRAPHICAL ABSTRACT

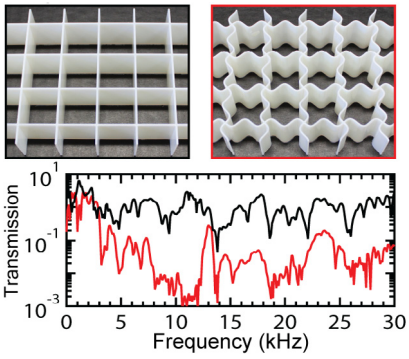

ARTICLE INFO

Article history:
Received 29 August 2017
Received in revised form 25 September 2017
Accepted 26 September 2017
Available online 4 October 2017

Keywords:
Metamaterials
Lattice materials
Vibration control
Band gaps
3D printing

ABSTRACT

Engineering the architectures of materials is a new approach to obtain unusual properties and functionalities in solids. Phononic crystals with periodically architected microstructures and compositions exhibit omnidirectional phononic band gaps, offering a unique capability to steer mechanical wave propagation. The coupled architecture-material design strategy, however, poses a significant challenge to design phononic crystals with broadband and multiband vibration control capabilities. Here we propose and demonstrate a new metamaterial design concept in which symmetry-broken ligaments with ordered topology are taken as the constitutive elements for regular lattice materials. Through integrative computational modeling, 3D printing, and vibration testing we demonstrate that the proposed lattice metamaterials can exhibit broad and multiple omnidirectional band gaps over a wide range of the geometry parameters that define the ligament. We show that the designed microstructure of the lattice metamaterial is robust and can be extended to baseline lattices with other topologies.

1. Introduction

Architected materials have gained significant interest within the research community in recent years due to their novel functionalities and unique properties that cannot be readily achieved in natural bulk solids. Architected materials have shown high specific stiffness [1–3], negative Poisson's ratio [4–8], negative thermal expansion [9–11], and unusual elastodynamic phenomena [12–14]. These unusual properties strongly depend upon the inherent architecture of these solids. An example of architected materials is the phononic crystal, which consists of periodically topological structures and materials dispersions. These rationally designed structures enable the manipulation of propagating acoustic and

* Corresponding author.
E-mail address: Lifeng.wang@stonybrook.edu (L. Wang).

https://doi.org/10.1016/j.eml.2017.09.012
2352-4316/

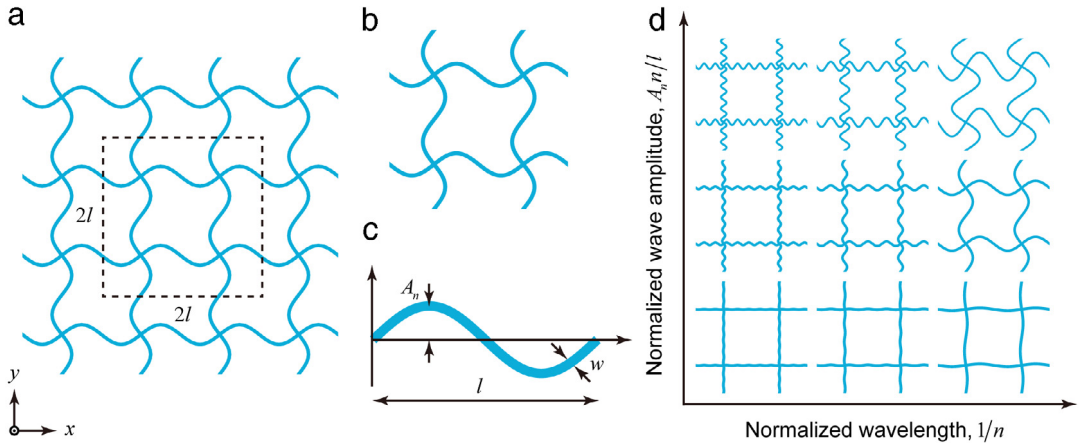

Fig. 1. Schematics of the proposed lattice metamaterials with curved ligaments. (a) Schematics of the lattice metamaterials. (b) Unit cell. (c) Sinusoidally-shaped ligament, and (d) Different unit cells in the $(1/n, A_n n/l)$ parameter space.

elastic waves or phonons [15,16]. The capability of tuning the wave propagation stems from the destructive interference at the interfaces of the periodic units. As a result, Bragg-type band gaps (i.e., frequency ranges where acoustic and elastic wave propagation are suppressed) arise in the dispersion relations of these architected materials [17,18]. Bragg-type band gaps offer a myriad of potential applications such as wave filtering [19,20], waveguiding [21,22], acoustic cloaking [17], thermal management [23–25], and energy harvesting [26–28].

Despite the fact that phononic crystals with architected structures and periodic assemblies have given ample evidence of their Bragg-type band gaps capability, the design of the architectures simply based on using monophase core material within a rigid unit cell topology poses a great challenge to obtain broad and multiple band gaps. The reason behind the limitation of the current architected materials design paradigm is the nature of Bragg scattering, which requires high lattice symmetry and contrast of mechanical impedance among the multiple components of the periodic assembly [29,30]. In this regard, lattice materials with engineered complex architectures have gained increasing attention, since the formation of phononic band gaps will only depend upon the lattice symmetry and the specific architectures used. Moreover, their design based on monophase cores allows producing lightweight phononic crystals with relatively simple fabrication procedures. Significant efforts have been devoted to exploring band gap properties in lattice materials with different topologies [31–38]. However, only triangular lattice configurations show a single locally resonant band gap [31]. To generate broad phononic band gaps in conventional lattice materials several design strategies have been proposed, including tuning the node connectivity [33], introducing local resonators [36,37], and using an external mechanical stimulus [39]. Although these studies have demonstrated the feasibility to achieve tunable band gaps, broad and multiple band gaps in conventional lattice materials are still largely not realized.

In this work, we demonstrate from numerical and experimental standpoints that broad and multiple phononic band gaps can be achieved in a new class of lattice metamaterials. Our metamaterials are created by replacing straight ligaments in conventional lattices with sinusoidally-shaped ligaments with specific wavelength order (Fig. 1). This metamaterial design concept is motivated by the observation that buckled-shape structures can be exploited to create tunable phononic band gaps [12,40]. Note that here we do not create the desired buckled lattice metamaterials using an external mechanical loading, because the short-wavelength buckling mode is never preferred for regular lattice metamaterials under macroscopic compression [41,42]. We first investigate the band gaps properties of the proposed lattice metamaterials by performing Bloch wave analysis in an infinitely periodic system. Low amplitude wave transmission tests are conducted on 3D printed samples to validate our model predictions. We show that the proposed metamaterial design concept is robust and efficient to generate broad and multiple band gaps. The metamaterial can be extended to curved ligaments with different amplitudes, wavelengths, aspect ratios, and other topologies.

2. Characterization of the lattice metamaterials

We begin by characterizing the proposed lattice metamaterial with a square topology, as schematically shown in Figs. 1(a)–(c). The sinusoidally-shaped ligaments can be mathematically described as:

$$y = A_n \sin\left(n\pi x/l\right), \tag{1}$$

where A_n is the wave amplitude, n is the number of half wavelengths, and l is the length of a regular straight beam. The length of the sinusoidally-shaped ligament is:

$$s = \int_0^l \sqrt{1 + \left(\frac{A_n n\pi}{l}\cos\left(\frac{n\pi x}{l}\right)\right)^2}\, dx, \tag{2}$$

Under the mass equivalence assumption, the width of the curved ligament beam can be calculated as

$$w = t \cdot l/s, \tag{3}$$

where t is the thickness of a regular ligament. For a given parameter $A_n n/l$ the width of the curved ligament is the same for any n. We therefore define two parameters to describe the curved ligament: the normalized wave amplitude $A_n n/l$ and normalized wavelength $1/n$. The shape of the unit cell in the parameters space is illustrated in Fig. 1(d).

For the following simulations and tests, the length and thickness of a regular ligament are $l = 2.25$ cm and $t = 0.1125$ cm $(l/t = 20)$ respectively unless otherwise specified. The out-of-the-plane thickness of each lattice metamaterial is $t_0 = 2.5$ cm. The lattice metamaterials are made of Verowhite (Stratasys, Ltd) with measured Young's modulus $E = 1.6$ GPa, Poisson's ratio $\nu = 0.33$, and density of $\rho = 1174$ kg m^{-3} (Fig. S1).

3. Broadband and multiband features of the lattice metamaterials

We first focus on lattice metamaterials with a square topology and investigate the effect of the ligament wavelength on the

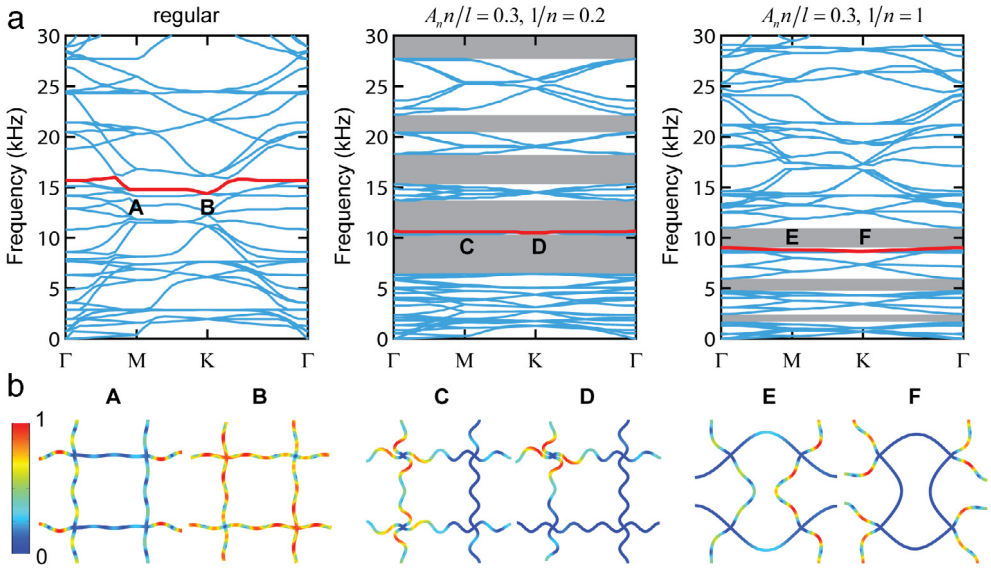

Fig. 2. Dispersion relations and eigenmodes of regular lattices and the proposed lattice metamaterials. (a) Dispersion relations for regular lattice material and lattice metamaterials with $A_n n/l = 0.3$, $1/n = 0.2$ and 1. (b) Eigenmodes at high-symmetry points of the first irreducible Brillouin zone. The gray-shaded regions indicate the phononic band gaps. (For interpretation of the references to color in this figure legend, the reader is referred to the web version of this article.)

dispersion relations by using the commercial finite element package COMSOL Multiphysics (See Supporting Information for details about the numerical simulation) [15,43,44]. Fig. 2(a) displays the phononic dispersion relations for a regular lattice material and lattice metamaterials with the same ligament amplitude ($A_n n/l = 0.3$) but different ligament wavelengths ($1/n = 0.2$ and 1). For the regular lattice material, no phononic band gaps can be observed, indicating that the elastic wave in the frequency ranges where the wavelength is comparable to the structural periodicity can freely propagate through the medium. These results agree with previous studies on wave propagation in conventional lattice materials [31]. By contrast, five complete band gaps emerge in the lattice metamaterial with a wavelength $1/n = 0.2$. When the ligament wavelength increases to $1/n = 1$, the width of the observed band gaps become smaller, or even tend to disappear – but still, three complete wave band gaps exist.

From a physical point of view, the formation of phononic band gaps can be attributed to Bragg scatterings and/or local resonances [13,18,29,30]. To gain insight into the fundamental mechanisms that govern the formation of the band gaps, we report in Fig. 2(b) the Bloch mode shapes at the high symmetry points **M** and **K** of the band edge (red line). In the case of a regular lattice material, the eigenmodes assume a global mode behavior that facilitates the travel of the phonons through the structure. By contrast, the eigenmodes corresponding to the lattice metamaterial with $1/n = 0.2$ and 1 being invested by wavenumber vectors directed to the **M** and **K** points show a strong localization behavior around the nodes. As a result, the energy associated with the propagating wave is trapped and localized in the lattice metamaterials, suggesting that broad omnidirectional band gaps are induced by local resonances. Further evidence of this omnidirectional band gap presence is also highlighted by the flatness of the red band edge, which indicates a nearly zero group velocity [45–47].

Low-frequency band gaps can also be observed in the lattice metamaterial with $1/n = 1$. To quantitatively understand the mechanisms responsible for these band gaps formation, we compare the effective wavelength with its structural periodicity. The effective Young's modulus and Poisson's ratio for the lattice metamaterials with $1/n = 1$ can be obtained by following a finite element procedure [48], which are 0.469 MPa and -0.65, respectively. Then, the transverse wave velocity for this lattice metamaterial can be calculated as $c_t = \sqrt{\mu^*/\rho^*}$, where μ^*(0.67 MPa) and ρ^*(115.6 kg m^{-3}) are the effective shear modulus and effective density, respectively. As a result, the estimated transverse velocities for $1/n = 1$ is 76.2 m s^{-1}. At the middle frequency of the lowest band gap, the effective wavelength is 3.75 cm, which is the same magnitude as the structural periodicity 4.5 cm. That means Bragg scattering is responsible for the low-frequency band gaps of lattice metamaterial with $1/n = 1$.

Our simulations and analyses indicate that the broadband and multiband features are due to the coexisting of two different mechanisms, i.e., local resonances and Bragg scattering. Intrinsically, the broad and multiple band gaps in the lattice metamaterials are dictated by the rational design of the ligament, which favors the coupling of the axial and bending motion [49].

4. Low amplitude wave transmission test

To validate the predictions of our models we have fabricated by 3D printing both regular lattices and lattice metamaterials with ligament amplitude $A_n n/l = 0.3$ and wavelength $1/n = 0.2$, 0.33 and 1 (Fig. S2 and Fig. 3 (a)). Each sample consisted of 2×5 unit cells and was made of Verowhite (Stratasys, Ltd). We have then performed low amplitude elastic wave transmission tests by exciting the 3D printed samples with an impact hammer (Figs. 3(b)–(c)). For details about the fabrication and experimental activity, the reader is referred to the Supporting Information. The transmission is computed as the ratio of output acceleration amplitude (a) to the input force amplitude (F). For the purpose of comparison, similar frequency domain analyses are also performed via numerical simulation to represent the wave propagation in finite-size structures (See Supporting Information for details of the numerical simulation) [45,50].

Figs. 3(d)–(g) show the transmission spectra of regular lattice material and lattice metamaterials with $1/n = 0.2$, 0.33, and 1, respectively. In the simulated transmission spectrum of the regular lattice material, one can observe several transmission dips that correspond to partial band gaps along **M–K** direction (Fig. 3(a)). In the transmission spectra of the lattice metamaterials, we notice the presence of attenuation zones that agree extremely well with the simulated phononic band gaps in the dispersion relations (Fig. 3(a)). By comparing the measured transmission spectra with the

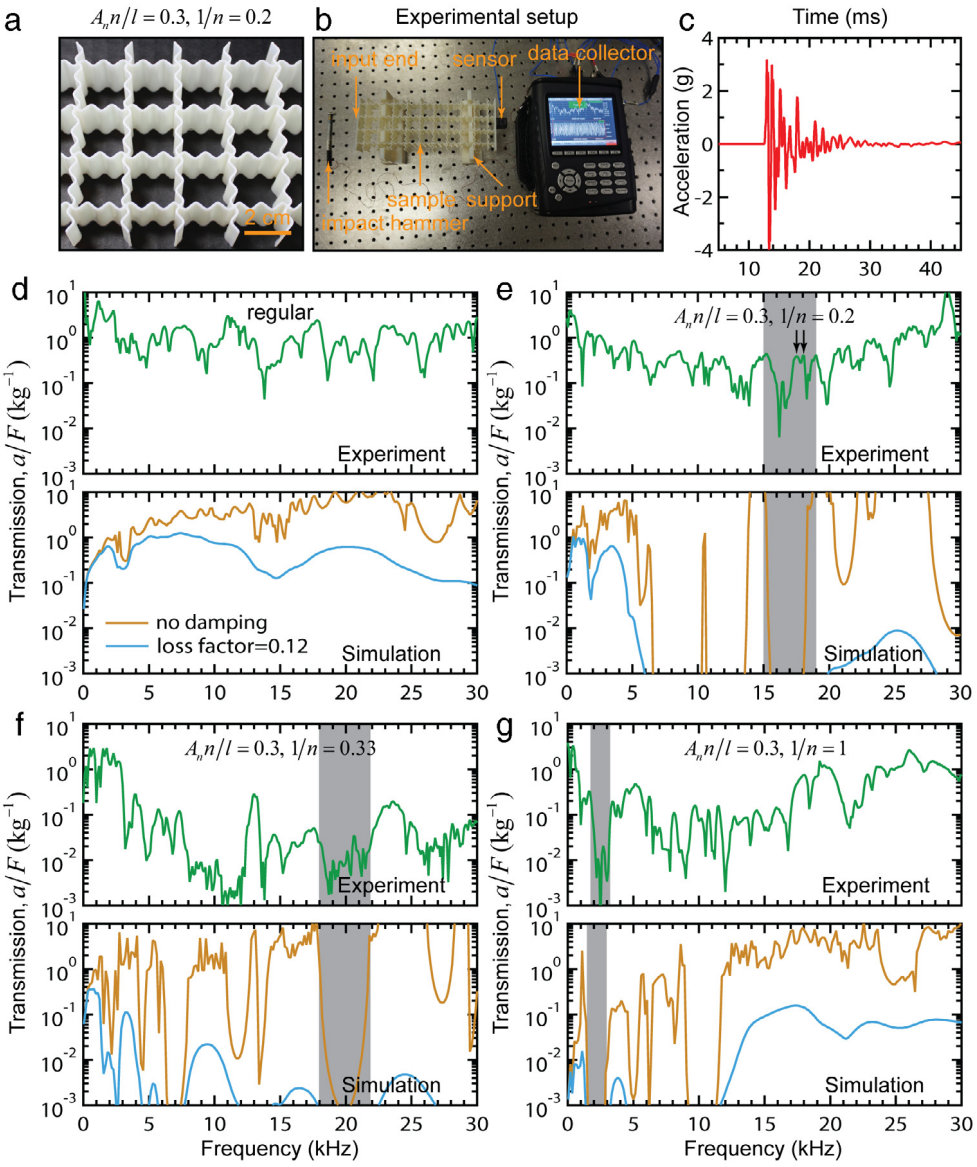

Fig. 3. Low amplitude wave transmission test of the lattice metamaterials along the **M–K** direction. (a) 3D printed samples with $A_n n/l = 0.3$, $1/n = 0.2$. (b) Experimental setup of the transmission test. (c) Measured acceleration–time curve for 3D-printed samples with $A_n n/l = 0.3$, $1/n = 0.2$. (d)–(g) Comparison between measured and simulated transmission spectra for lattice metamaterials with different wavelengths. The gray-shaded regions indicate the phononic band gaps. (For interpretation of the references to color in this figure legend, the reader is referred to the web version of this article.)

predictions from the model we notice that simulated attenuation zones can be identified within the measured transmission spectra. For lattice metamaterials with$1/n = 1$, a quantitative agreement for the transmissibility values can be observed for the partial band gaps within 1.44 kHz –2.94 kHz. A predicted partial band gap between 15 kHz and 19 kHz (along **M-K** direction, gray-shaded region) can be clearly seen for lattice metamaterials with$1/n = 0.2$. To better understand the wave propagation in the lattice metamaterials we plot in Fig. 4 the dynamic response of the metamaterials under harmonic excitation inside and outside the band gaps. For both lattice metamaterials, the incident plane waves inside the band gaps decay rapidly, whereas incident waves can travel through the metamaterials when the excitation frequency lies outside the band gaps.

It is noticeable that the simulated partial band gaps over the whole sweeping frequency range cannot be perfectly captured using the transmission test. For example, the simulated partial band gap for the lattice metamaterial with $1/n = 0.2$ is between 15 kHz and 19 kHz, while transmission peaks arise in the measured transmission spectra for the same frequency range (black arrows). This discrepancy could be associated with one, or a combination of the following factors: (1) Boundary conditions. In the simulation, we use perfectly matched layers to prevent reflections by the scattering waves from the domain boundaries, while this virtual boundary condition cannot be realized in a lab environment. (2) Out-of-the-plane vibration. In our simulations, the plane strain condition is adopted for the lattice metamaterials. Out-of-the-plane vibration could, however, exist in the finite-thickness lattice metamaterials. (3) The anisotropic feature of the samples fabricated by 3D printing. Due to the layer by layer manufacture process of 3D printing, the mechanical properties of the printed samples strongly depend on the printing directions. While in our numerical simulations, an isotropic material model is adopted [51]. (4) Damping effect. Most of the polymers for 3D printing have a significant damping effect [52], which could attenuate the response and minimize the effect of the phononic band gaps. We are unable to quantitatively and separately understand the contribution of each possible reason

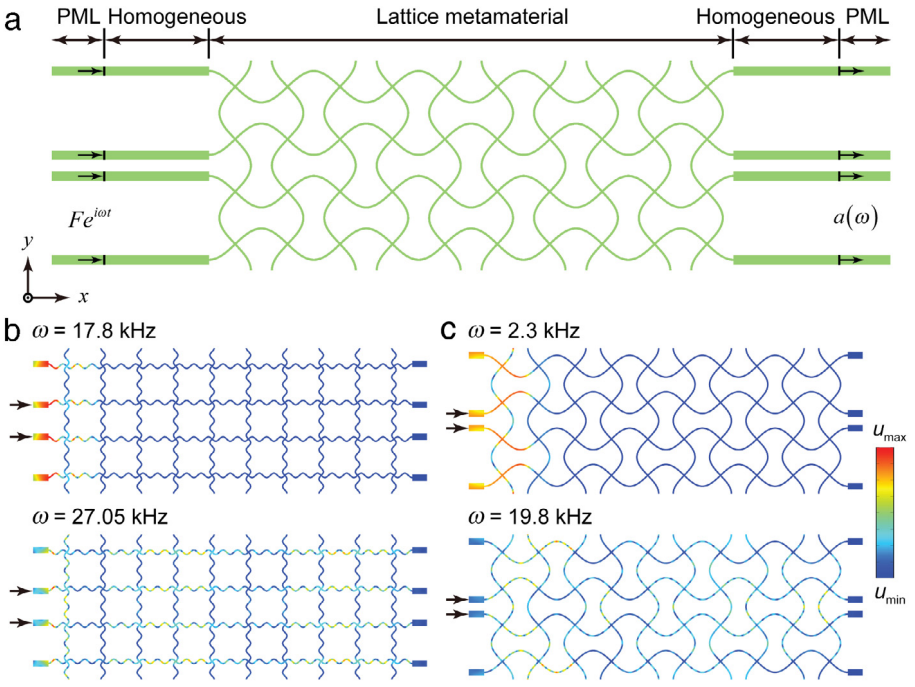

Fig. 4. Frequency domain analysis for low amplitude wave transmission. (a) FE model (See Supporting Information for details). (b)–(c) Dynamic response of the lattice metamaterials at a frequency inside and outside the band gaps for lattice metamaterials with $A_n n/l = 0.3$, $1/n = 0.2$ and $A_n n/l = 0.3$, $1/n = 1$. (For interpretation of the references to color in this figure legend, the reader is referred to the web version of this article.)

for the discrepancy, but the effect of damping on the vibration can be understood. To this end, we have first conducted DMA test to characterize the damping feature of Verowhite. It is noticeable that at room temperature (23 °C), the loss factor is about 0.12 (Figure S2), which will be used in the frequency domain analysis. Then, we have conducted frequency domain analysis to study the effect of damping on the transmission properties, as shown in Fig. 3. For example, when damping effect is incorporated in our simulations, there is significant attenuation in a high-frequency range (>5 kHz), which agreed better with the measured transmission spectra. While at low-frequency range, damping effect can be neglected. These simulations can partially explain that damping effect plays a significant role in our experiments. Notwithstanding these limitations, the low amplitude wave transmission test of the finite-size lattice metamaterials is able to indicate the presence of the broadband and multiband absorption feature.

5. Effect of geometric features and topologies

5.1. Effects of the ligament geometry on the vibration control

We have numerically and experimentally demonstrated that broad and multiple band gaps can be obtained in the proposed lattice metamaterials. This remarkable vibration control capability is intrinsically dictated by the artificially architected ligament with a curved shape. We then systematically investigate the effects of the geometric features of the curved beam, i.e., $A_n n/l$ and $1/n$, over the band gap properties. To this end, we define two indicators to characterize the broadband and multiband features: the maximum relative band gaps $(\Delta\omega/\omega_*)_{\max}$ and the total relative band gaps $\sum(\Delta\omega/\omega_*)$. The two metrics are defined by $\Delta\omega$ (band gap width) and the midgap frequency ω_* [15]. Figs. 5(a) and (b) show the evolution of the maximum band gap and total band gaps as a function of the geometric features. For a given ligament wavelength both broad and multiple band gaps increase proportionally to the ligament wave amplitude. For extremely small ligament amplitudes ($A_n n/l = 0.05$), no complete band gaps can be observed (Fig. 5(c)). This is expected since no complete band gaps exist in regular lattice materials with square topology. It is also noticeable that the broad and multiple band gaps arise in lattice metamaterials with the largest wave amplitude and a wavelength range from 0.4 to 0.8 (Fig. 5(d)).

Another geometric parameter of interest is the beam slenderness ratio, which dictates the deformation behavior of the ligament. Here for simplicity, we use l/t to examine the effect of slenderness ratio on the band gap property. Figs. 6(a)–(b) show the evolution of the maximum and total band gaps as a function of l/t for lattice metamaterials with $1/n = 0.25$ and $1/n = 0.5$. For the purpose of the comparison, the evolution of the band gaps related to regular lattice materials with different slenderness ratios is also presented. As expected, no complete or small band gaps can be observed in the regular lattice materials. By contrast, for lattice metamaterials with different wavelengths, broad and multiple band gaps can be observed. Specifically, for the lattice metamaterial with $1/n = 0.25$, an optimal maximum band gap is observed for a $l/t = 10$, while for lattice metamaterials with $1/n = 0.5$, the maximum band gap is proportional to l/t (Figs. 6(c) and (d)). It is also interesting to notice that the higher the waviness, the higher is the maximum band gap, especially for l/t lower than 30. High waviness ($1/n = 0.25$ in this case) allows obtaining maximum band gaps even at relatively low slenderness ratios, for which shear deformation of the cross section becomes more important. On the contrary, lower waviness metamaterials tend to feature low maximum band gaps for thicker ligaments. It should be pointed out that the evolution of the maximum band gaps for $1/n = 0.25$ does not monotonically increase. The reasons are twofold: (1) the maximum band gap for each slenderness ratio is taken from the dispersion relations and therefore may not exist at the same bands. The evolution of a single band gap is not tracked because the maximum band gaps are more important in practical applications. (2) All numerical simulations suggest that there is no an obvious trend for the evolution of band gaps as a function of geometric features such as ligament wave amplitude and wavelength. In the case of the total band gaps, it is evident

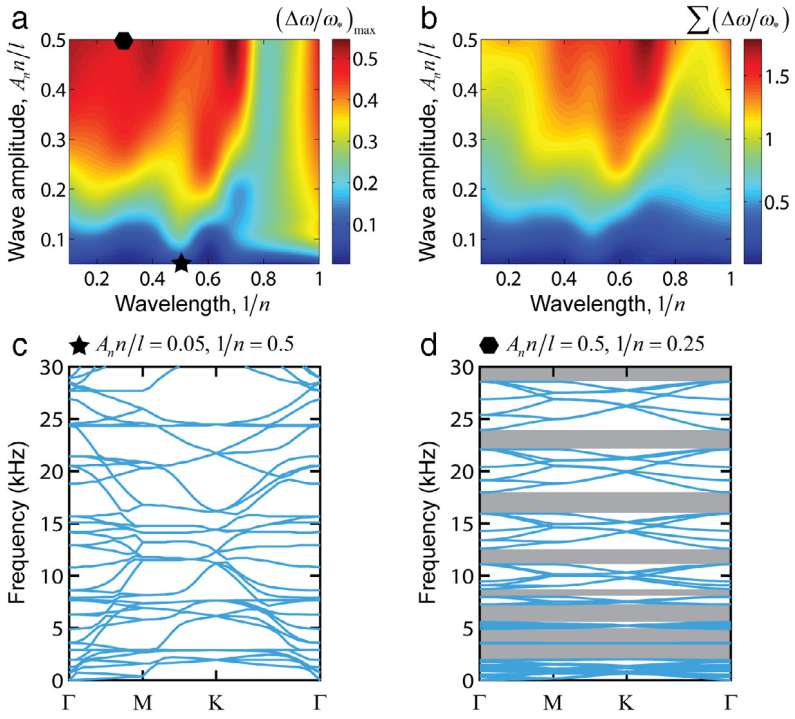

Fig. 5. Effects of the ligament geometry on the phononic band gaps. (a)–(b) Effects of the wavelength and wave amplitude on the evolution of the maximum and full band gaps. (c)–(d) Dispersion relations for the lattice metamaterials with two extreme ligament amplitudes, $A_n n/l = 0.05$, $1/n = 0.5$ and $A_n n/l = 0.5$, $1/n = 0.25$. The gray-shaded regions indicate the phononic band gaps. (For interpretation of the references to color in this figure legend, the reader is referred to the web version of this article.)

the direct proportionality with increasing values of l/t, although the amount of the total band gap tends to plateau for very high ligaments slenderness. The relative density of lattice materials is inversely proportional to the slenderness ratio [53], and this indicates that the proposed lattice metamaterials not only exhibit broad and multiple band gap features, but are also lightweight.

These systematic investigations reveal that the geometric features of the curved ligaments (amplitude, wavelength, and slenderness ratio) are critical to the formation of band gaps. Although we have not built any analytical relation between these geometric features with the band gap properties of the lattice metamaterials, it is evident that the geometry uniquely dictates the deformation behavior and the vibrational modes of the artificially designed ligament. Quite importantly, these parameters can be tailored to design lattice metamaterials with desired or optimized vibration control capability.

5.2. Effect of lattice topology on the vibration control

While the results reported so far are focused on lattice metamaterials with a square topology, we now proceed to demonstrate that the proposed lattice metamaterial design is not restricted to this specific topology only, and can be extended to lattice metamaterials with other shapes. Due to the geometric constraints in triangular lattice metamaterials and for the purpose of comparison, here we focus on lattice metamaterials with even numbers of half sinusoid, i.e., $n = 2$ and 4. We first report the simulated dispersion relations for lattice metamaterials with different topologies in Figs. 7 (a)–(b). As expected, broad and multiple band gaps persist in each lattice metamaterials defined by different topologies, giving evidence that this design concept is general and robust. This phenomenon is quite different from that observed in conventional lattice materials, whose band gap properties strongly depend on the lattice topologies or the node connectivity [54]. We further

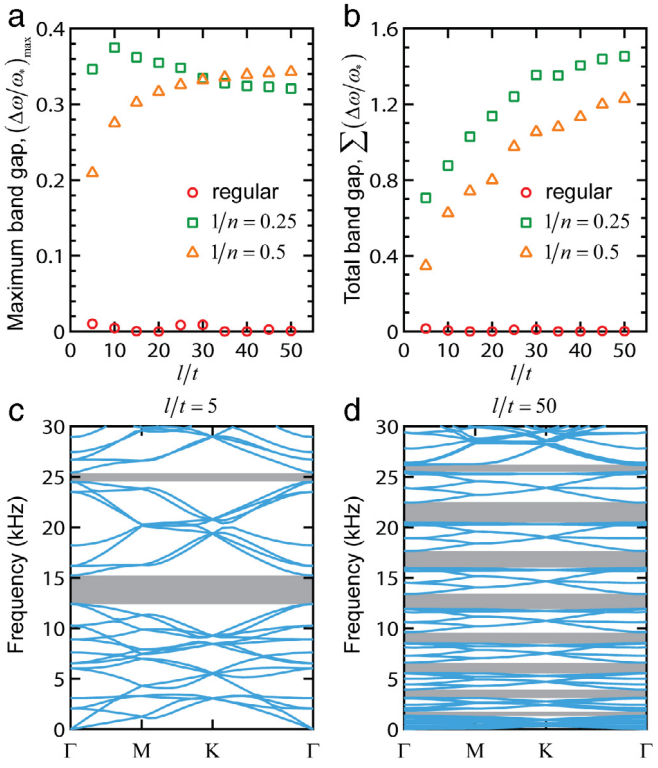

Fig. 6. Effect of the slenderness of the ligament on the evolution of the phononic band gaps. (a)–(b) Evolution of the maximum and total band gaps with respect to the ligament slenderness l/t. (c)–(d) Dispersion relations for the lattice metamaterials with extreme slenderness, $l/t = 5$ and $l/t = 50$. Here $A_n n/l = 0.30$ and $1/n = 0.5$. The gray-shaded regions indicate the phononic band gaps. (For interpretation of the references to color in this figure legend, the reader is referred to the web version of this article.)

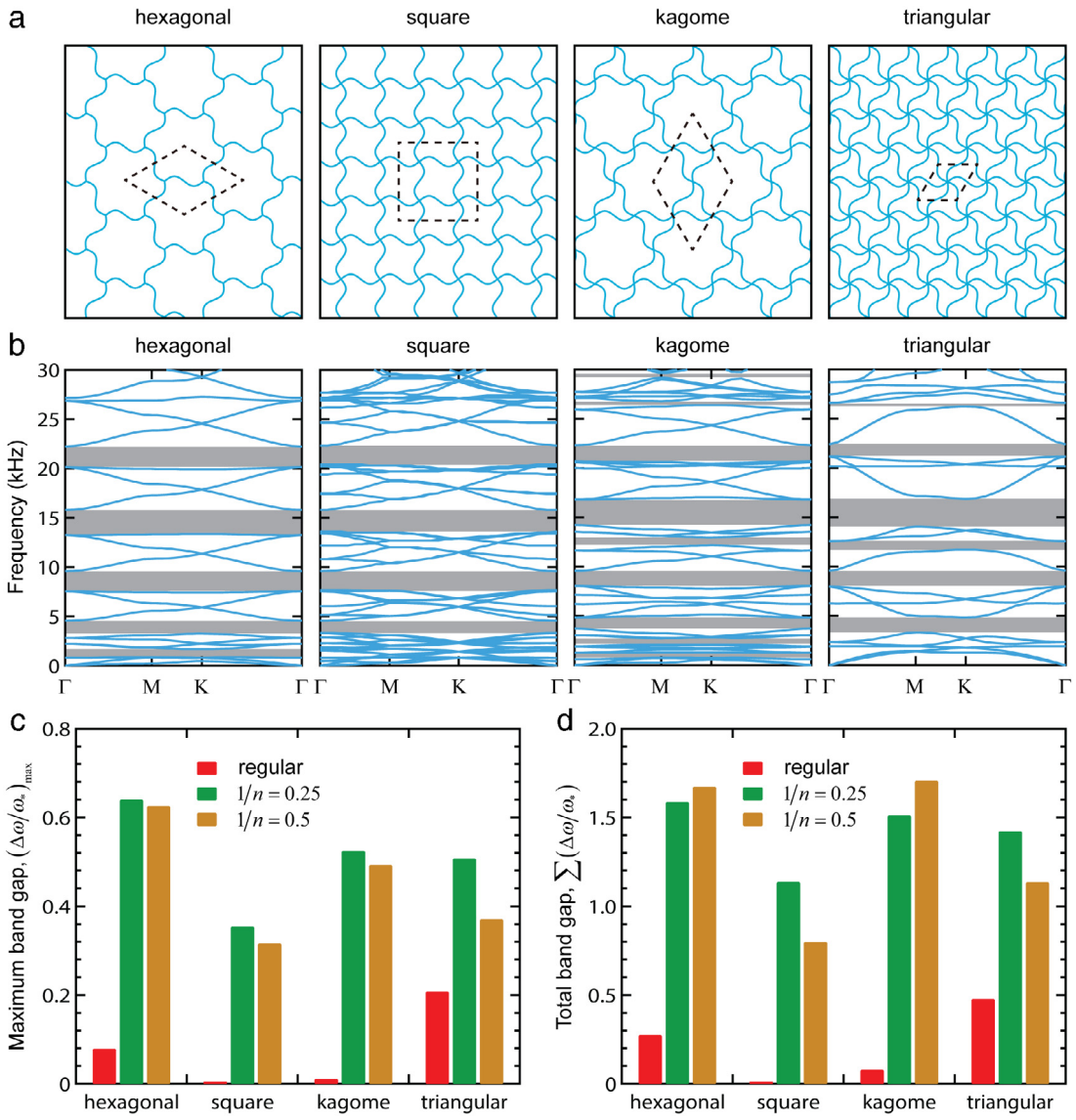

Fig. 7. Effect of lattice topology on phononic band gaps. (a) Schematics of lattice metamaterials with hexagonal, square, kagome, and triangular topologies, respectively. The area surrounded by the dash lines is the representative unit cell for each topology. (b) Dispersion relations for lattice metamaterials with hexagonal, square, kagome, and triangular topologies. Here each ligament has a wave amplitude of$A_n n/l = 0.30$ and wavelength of $1/n = 0.5$. (c)–(d) Maximum band gap and total band gaps for lattice metamaterials with hexagonal, square, kagome, and triangular topologies. Here each ligament has a wave amplitude of$A_n n/l = 0.30$ but different wavelengths. The gray-shaded regions indicate the phononic band gaps. (For interpretation of the references to color in this figure legend, the reader is referred to the web version of this article.)

compare the maximum and total band gaps for lattice metamaterials with different topologies and different wavelengths (Figs. 7 (c)–(d)). It can be seen that both maximum and total band gaps for lattice metamaterials are larger than those of regular lattice materials. Note that for a given topology, a combination of optimal ligament wavelength and wave amplitude is essential to generate the complete band gaps, as these geometric parameters intrinsically dictate the vibrational modes of ligaments.

To validate the numerical predictions, low amplitude wave transmission tests along the **M-K** direction are performed on 3D-printed lattice metamaterials with hexagonal, square, kagome, and triangular topologies (Fig. 8(a) and Fig. S3). It is worth noticing the very good agreement with the measured transmission spectra, especially at low frequencies. By using the sinusoidally-shaped ligament microstructure topology one can seize new opportunities to design metamaterial systems that can integrate geometric features at different microstructural levels, i.e., the architecture of the ligament and the topology of the lattice metamaterials.

6. Conclusions

We have proposed and demonstrated the existence of a new class of lattice metamaterials consisting of curved ligaments that possess both broad and multiple phononic band gaps. These remarkable band gap properties are intrinsically controlled by the unique vibration behavior of the artificially designed ligaments. Moreover, our results indicate that the proposed metamaterial design concept not only works for a wide range of geometric parameters of the curved ligaments, but can also be extended to other topologies. Unlike conventional phononic crystals with multiple elastic phases, the broad and multiple band gap properties of the lattice metamaterials proposed in this work are material-independent, which indicates that a coupled material-architecture design strategy is not essential. However for higher amplitude wave, such as impact or shock wave, both architectures and constitutive materials are critical to the dynamic response of the lattice metamaterials. Furthermore, the proposed metamaterial design

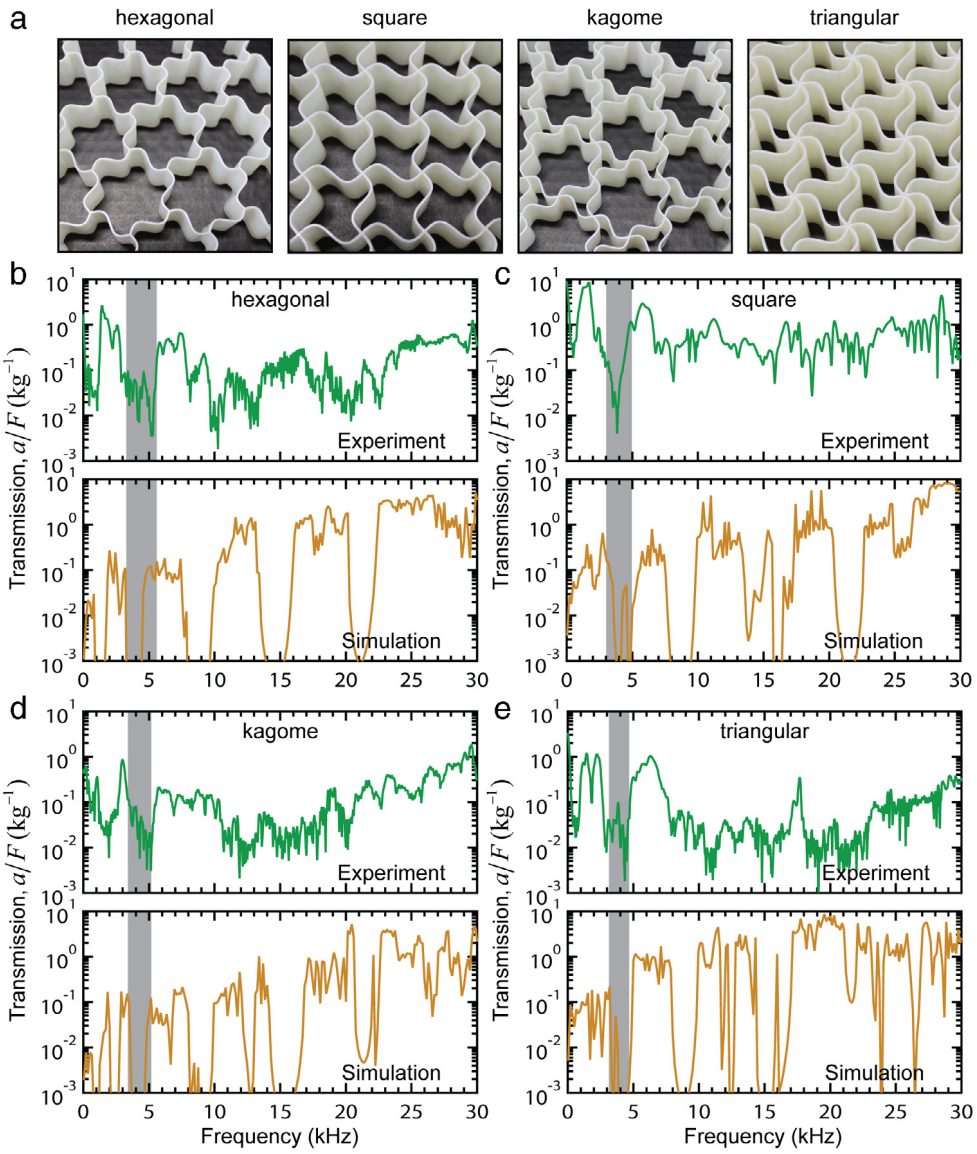

Fig. 8. Wave transmission test of the lattice metamaterials with different topologies along the **M–K** direction. (a) 3D printed lattice metamaterials with hexagonal, square, kagome, and triangular topologies. (b)–(e) Comparison between measured and simulated transmission spectra for lattice metamaterials with different topologies. Here each ligament has a wave amplitude of$A_n n/l = 0.30$ and wavelength of $1/n = 0.5$. The out-of-the-plane thickness of each lattice metamaterial is 2.5 cm. The gray-shaded regions indicate the phononic band gaps. (For interpretation of the references to color in this figure legend, the reader is referred to the web version of this article.)

concept is scale-independent and can be applied to various length scales. Due to the frequency range limitation of our vibration transmissibility test, we have fabricated samples with a ligament length of 2.25 cm and made of Verowhite polymer as demonstrators. Similar phononic band gap properties within different frequency ranges can be however envisioned for lattice metamaterials at various length scales. Finally, the prescribed curvature in the architected ligaments can be harnessed to tailor the band gap properties. The curved ligaments have excellent stretchability under tension because the local strain is much smaller than the macroscopic one when the lattice metamaterials are subjected to uniaxial stretching. As a result, the external mechanical stimulus of low magnitude could be further imposed to dynamically tune the band gaps. The metamaterial design concept proposed here provides new insights into the development of architected metamaterials with a broad range of potential applications, such as wave filtering, waveguiding, programmable acoustic metamaterials, vibration isolation, as well as stretchable electronics.

Acknowledgments

The authors gratefully acknowledge the financial support from the National Science Foundation (CMMI-1437449, CMMI-1462270), the Region 2 University Transportation Research Center (UTRC-49198-35-28), and the Office of Naval Research. The authors are also grateful to Prof. Katia Bertoldi (Harvard University) for inspirational discussions. Y. Chen thanks Dr. Pu Zhang (The University of Manchester) for helpful discussion and Belle Zhou for her help in photographing the 3D printed samples.

Appendix A. Supplementary data

Supplementary material related to this article can be found online at https://doi.org/10.1016/j.eml.2017.09.012.

References

[1] T.A. Schaedler, A.J. Jacobsen, A. Torrents, A.E. Sorensen, J. Lian, J.R. Greer, L. Valdevit, W.B. Carter, Ultralight metallic microlattices, Science 334 (2011) 962.

[2] X.Y. Zheng, H. Lee, T.H. Weisgraber, M. Shusteff, J. DeOtte, E.B. Duoss, J.D. Kuntz, M.M. Biener, Q. Ge, J.A. Jackson, S.O. Kucheyev, N.X. Fang, C.M. Spadaccini, Ultralight, ultrastiff mechanical metamaterials, Science 344 (2014) 1373.
[3] X.Y. Zheng, W. Smith, J. Jackson, B. Moran, H.C. Cui, D. Chen, J.C. Ye, N. Fang, N. Rodriguez, T. Weisgraber, C.M. Spadaccini, Multiscale metallic metamaterials, Nature Mater. 15 (2016) 1100.
[4] T.A. Hewage, K.L. Alderson, A. Alderson, F. Scarpa, Double-negative mechanical metamaterials displaying simultaneous negative stiffness and negative Poisson's ratio properties, Adv. Mater. 28 (2016) 10323.
[5] K. Bertoldi, P.M. Reis, S. Willshaw, T. Mullin, Negative Poisson's ratio behavior induced by an elastic instability, Adv. Mater. 22 (2010) 361.
[6] S. Babaee, J. Shim, J.C. Weaver, E.R. Chen, N. Patel, K. Bertoldi, 3D soft metamaterials with negative Poisson's ratio, Adv. Mater. 25 (2013) 5044.
[7] A. Clausen, F.W. Wang, J.S. Jensen, O. Sigmund, J.A. Lewis, Topology optimized architectures with programmable Poisson's ratio over large deformations, Adv. Mater. 27 (2015) 5523.
[8] J.N. Grima, S. Winczewski, L. Mizzi, M.C. Grech, R. Cauchi, R. Gatt, D. Attard, K.W. Wojciechowski, J. Rybicki, Tailoring graphene to achieve negative Poisson's ratio properties, Adv. Mater. 27 (2015) 1455.
[9] Q.M. Wang, J.A. Jackson, Q. Ge, J.B. Hopkins, C.M. Spadaccini, N.X. Fang, Lightweight mechanical metamaterials with tunable negative thermal expansion, Phys. Rev. Lett. 117 (2016) 175901.
[10] L. Ai, X.-L. Gao, Metamaterials with negative Poisson's ratio and non-positive thermal expansion, Compos. Struct. 162 (2017) 70.
[11] H. Xu, D. Pasini, Structurally efficient three-dimensional metamaterials with controllable thermal expansion, Sci. Rep. 6 (2016) 34924.
[12] P. Wang, F. Casadei, S.C. Shan, J.C. Weaver, K. Bertoldi, Harnessing buckling to design tunable locally resonant acoustic metamaterials, Phys. Rev. Lett. 113 (2014) 014301.
[13] Y.Y. Chen, L.F. Wang, Periodic co-continuous acoustic metamaterials with overlapping locally resonant and Bragg band gaps, Appl. Phys. Lett. 105 (2014) 191907.
[14] K.H. Matlack, A. Bauhofer, S. Krodel, A. Palermo, C. Daraio, Composite 3D-printed metastructures for low-frequency and broadband vibration absorption, Proc. Natl. Acad. Sci. USA 113 (2016) 8386.
[15] A. Khelif, B. Aoubiza, S. Mohammadi, A. Adibi, V. Laude, Complete band gaps in two-dimensional phononic crystal slabs, Phys. Rev. E 74 (2006) 046610.
[16] M.S. Kushwaha, P. Halevi, G. Martinez, L. Dobrzynski, B. Djafarirouhani, Theory of acoustic band-structure of periodic elastic composites, Phys. Rev. B 49 (1994) 2313.
[17] M. Maldovan, Sound and heat revolutions in phononics, Nature 503 (2013) 209.
[18] Y. Achaoui, A. Khelif, S. Benchabane, L. Robert, V. Laude, Experimental observation of locally-resonant and Bragg band gaps for surface guided waves in a phononic crystal of pillars, Phys. Rev. B 83 (2011) 104201.
[19] P. Zhang, A.C. To, Broadband wave filtering of bioinspired hierarchical phononic crystal, Appl. Phys. Lett. 102 (2013) 121910.
[20] Y. Pennec, B. Djafari-Rouhani, J.O. Vasseur, A. Khelif, P.A. Deymier, Tunable filtering and demultiplexing in phononic crystals with hollow cylinders, Phys. Rev. E 69 (2004) 046608.
[21] A. Khelif, P.A. Deymier, B. Djafari-Rouhani, J.O. Vasseur, L. Dobrzynski, Two-dimensional phononic crystal with tunable narrow pass band: Application to a waveguide with selective frequency, J. Appl. Phys. 94 (2003) 1308.
[22] A. Khelif, A. Choujaa, S. Benchabane, B. Djafari-Rouhani, V. Laude, Guiding and bending of acoustic waves in highly confined phononic crystal waveguides, Appl. Phys. Lett. 84 (2004) 4400.
[23] N. Zen, T.A. Puurtinen, T.J. Isotalo, S. Chaudhuri, I.J. Maasilta, Engineering thermal conductance using a two-dimensional phononic crystal, Nature Commun. 5 (2014) 3435.
[24] J.K. Yu, S. Mitrovic, D. Tham, J. Varghese, J.R. Heath, Reduction of thermal conductivity in phononic nanomesh structures, Nature Nanotechnol. 5 (2010) 718.
[25] M. Maldovan, Narrow low-frequency spectrum and heat management by thermocrystals, Phys. Rev. Lett. 110 (2013) 025902.
[26] H.Y. Lv, X.Y. Tian, M.Y. Wang, D.C. Li, Vibration energy harvesting using a phononic crystal with point defect states, Appl. Phys. Lett. 102 (2013) 034103.
[27] L.Y. Wu, L.W. Chen, C.M. Liu, Acoustic energy harvesting using resonant cavity of a sonic crystal, Appl. Phys. Lett. 95 (2009) 013506.
[28] S. Gonella, A.C. To, W.K. Liu, Interplay between phononic bandgaps and piezoelectric microstructures for energy harvesting, J. Mech. Phys. Solids 57 (2009) 621.
[29] Z. Liu, X. Zhang, Y. Mao, Y. Zhu, Z. Yang, C. Chan, P. Sheng, Locally resonant sonic materials, Science 289 (2000) 1734.
[30] Z.Y. Liu, C.T. Chan, P. Sheng, A.L. Goertzen, J.H. Page, Elastic wave scattering by periodic structures of spherical objects: Theory and experiment, Phys. Rev. B 62 (2000) 2446.
[31] A.S. Phani, J. Woodhouse, N. Fleck, Wave propagation in two-dimensional periodic lattices, J. Acoust. Soc. Am. 119 (2006) 1995.
[32] S. Krodel, C. Daraio, Microlattice metamaterials for tailoring ultrasonic transmission with elastoacoustic hybridization, Phys. Rev. Appl. 6 (2016) 064005.
[33] P. Wang, F. Casadei, S.H. Kang, K. Bertoldi, Locally resonant band gaps in periodic beam lattices by tuning connectivity, Phys. Rev. B 91 (2015) 020103.
[34] Y. Chen, L. Wang, Harnessing structural hierarchy to design stiff and lightweight phononic crystals, Extreme Mech. Lett. 9 (2016) 91.
[35] D. Mousanezhad, S. Babaee, R. Ghosh, E. Mahdi, K. Bertoldi, A. Vaziri, Honeycomb phononic crystals with self-similar hierarchy, Phys. Rev. B 92 (2015) 104304.
[36] S. Krödel, T. Delpero, A. Bergamini, P. Ermanni, D.M. Kochmann, 3D auxetic microlattices with independently controllable acoustic band gaps and quasi-static elastic moduli, Adv. Energy Mater. 16 (2014) 357.
[37] C. Yilmaz, G.M. Hulbert, N. Kikuchi, Phononic band gaps induced by inertial amplification in periodic media, Phys. Rev. B 76 (2007) 054309.
[38] L.F. Wang, K. Bertoldi, Mechanically tunable phononic band gaps in three-dimensional periodic elastomeric structures, Int. J. Solids Struct. 49 (2012) 2881.
[39] M. Alkhader, S. Iyer, W.X. Shi, T.A. Venkatesh, Low frequency acoustic characteristics of periodic honeycomb cellular cores: The effect of relative density and strain fields, Compos. Struct. 133 (2015) 77.
[40] S. Rudykh, M.C. Boyce, Transforming wave propagation in layered media via instability-induced interfacial wrinkling, Phys. Rev. Lett. 112 (2014) 034301.
[41] N. Ohno, D. Okumura, T. Niikawa, Long-wave buckling of elastic square honeycombs subject to in-plane biaxial compression, Int. J. Mech. Sci. 46 (2004) 1697.
[42] B. Haghpanah, J. Papadopoulos, D. Mousanezhad, H. Nayeb-Hashemi, A. Vaziri, Buckling of regular chiral and hierarchical honeycombs under a general macroscopic stress state, Proc. R. Soc. A 470 (2014).
[43] M. Maldovan, E.L. Thomas, Periodic Materials and Interference Lithography: For Photonics, Phononics and Mechanics, John Wiley & Sons, 2009.
[44] J. Achenbach, Wave Propagation in Elastic Solids, Elsevier, 2012.
[45] A. Khelif, Y. Achaoui, S. Benchabane, V. Laude, B. Aoubiza, Locally resonant surface acoustic wave band gaps in a two-dimensional phononic crystal of pillars on a surface, Phys. Rev. B 81 (2010) 214303.
[46] C. Goffaux, J. Sánchez-Dehesa, Two-dimensional phononic crystals studied using a variational method: application to lattices of locally resonant materials, Phys. Rev. B 67 (2003) 144301.
[47] G. Wang, D.L. Yu, J.H. Wen, Y.Z. Liu, X.S. Wen, One-dimensional phononic crystals with locally resonant structures, Phys. Lett. A 327 (2004) 512.
[48] Y. Chen, T. Li, F. Scarpa, L. Wang, Lattice metamaterials with mechanically tunable poisson's ratio for vibration control, Phys. Rev. Appl. 7 (2017) 024012.
[49] G. Trainiti, J.J. Rimoli, M. Ruzzene, Wave propagation in periodically undulated beams and plates, Int. J. Solids Struct. 75–76 (2015) 260.
[50] W. Chew, Q. Liu, Perfectly matched layers for elastodynamics: A new absorbing boundary condition, J. Comput. Acoust. 4 (1996) 341.
[51] P. Zhang, A.C. To, Transversely isotropic hyperelastic-viscoplastic model for glassy polymers with application to additive manufactured photopolymers, Int. J. Plast. 80 (2016) 56.
[52] P. Zhang, M.A. Heyne, A.C. To, Biomimetic staggered composites with highly enhanced energy dissipation: Modeling, 3D printing, and testing, J. Mech. Phys. Solids 83 (2015) 285.
[53] L. Gibson, M. Ashby, Cellular Solids: Structure and Properties, Cambridge University Press, 1997.
[54] P. Wang, F. Casadei, S.H. Kang, K. Bertoldi, Locally resonant band gaps in periodic beam lattices by tuning connectivity, Phys. Rev. B 91 (2015) 020103.